Measurement of the refractive index of human teeth by optical coherence tomography

Zhuo Meng
X. Steve Yao
Tianjin University
College of Precision Instrument and Opto-electronics
    Engineering
Optical Polarization Research Center
    and
Key Laboratory of Opto-electronics Information Science
    and Technology of Ministry of Education
Tianjin 300072, China

Hui Yao
Tianjin Stomatological Hospital
Research Center
Tianjin 300041
China

Yan Liang
Tiegen Liu
Tianjin University
College of Precision Instrument and Opto-electronics
    Engineering
Optical Polarization Research Center
    and
Key Laboratory of Opto-electronics Information Science
    and Technology of Ministry of Education
Tianjin 300072, China

Yanni Li
Guanhua Wang
Tianjin Stomatological Hospital
Research Center
Tianjin 300041
China

Shoufeng Lan
Tianjin University
College of Precision Instrument and Opto-electronics
    Engineering
Optical Polarization Research Center
    and
Key Laboratory of Opto-electronics Information Science
    and Technology of Ministry of Education
Tianjin 300072, China

Address all correspondence to: Zhuo Meng, College of Precision Instrument & Opto-electronics Engineering, Tianjin University, 92, Weijin Road, Nankai District-Tianjin, Tianjin 300072 China; Tel: 86–022–27409621; Fax: 86–022–27400285; E-mail: tjictom@gmail.com

Abstract. We describe a novel method based on optical coherence tomography (OCT) for the accurate measurement of the refractive index of *in vitro* human teeth. We obtain the refractive indices of enamel, dentin, and cementum to be 1.631 ± 0.007, 1.540 ± 0.013, and 1.582 ± 0.010, respectively. The profile of the refractive index is readily obtained via an OCT B scan across a tooth. This method can be used to study the refractive index changes caused by dental decay and therefore has great potential for the clinical diagnosis of early dental caries. © *2009 Society of Photo-Optical Instrumentation Engineers.* [DOI: 10.1117/1.3130322]

1 Introduction

Optical coherence tomography (OCT) is a novel biological imaging technology that has been developed rapidly in the last decade. Since Huang et al. obtained the first OCT image of the tiny structure of the human retina in 1991,[1] many research groups have achieved clear OCT images of both normal and decayed dental tissues and have proven that OCT can be applied to oral medical diagnosis.[2–4]

The refractive index is an important optical parameter of biological tissues, especially for teeth. It has been found that early demineralization caused by caries will alter a tooth's refractive index; therefore, the accurate measurement of the changes in a tooth's refractive index can help the early diagnosis of dental caries.[5] Presently, a relatively successful method for measuring a tooth's refractive index is the OCT-based focus-tracing method.[6–8] However, such a measurement is difficult to perform in practice because it requires at least two adjustments of the focal point during each measurement and the precise calibration of the numerical aperture of the lens, making the measurement slow and more susceptible to measurement errors. A method to record spatial variations of the refractive index of the porcine renal artery using differential-phase optical coherence microscopy was reported in Ref. 9. However, the calculation of the tissue refractive index requires a priori knowledge of the section thickness and the refractive index of the surrounding medium. Another limitation of this method is that the thickness of the calcite prism pair should be carefully adjusted to introduce the same amount of equivalent phase retardation introduced by the tissue.

This paper describes a simple method based on optical path-length (OPL) matching during an OCT scan for measuring the refractive index of the *in vitro* teeth. This OCT path-length matching method has the advantages of easy operation, fast measurement, and high accuracy, especially compared
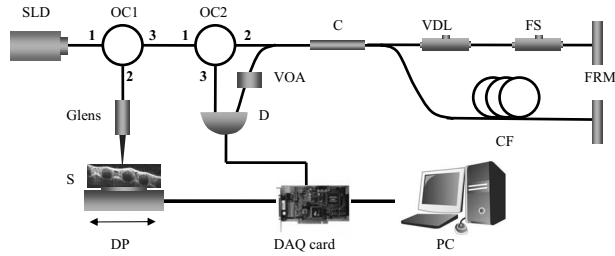
Fig. 1 Schematic of the all-fiber OCT system. SLD: superluminescent diode; OC: optical circulator; Glens: GRIN lens; S: sample, DP: displacement plate; C: coupler; D: detector; VDL: variable delay line; FS: fiber stretcher; FRM: Faraday rotator mirror; CF: compensation fibers; VOA: variable optical attenuation; DAQ card: data acquisition card; PC: personal computer.

with the OCT focus-tracing method. As a result, the index distribution profile across a tooth also can be readily obtained. In this paper, we first present the basic structure of our all-fiber polarization-insensitive OCT system, and then describe the principle of the path-length matching method. Finally, we show the measurement results of the refractive indices of different parts of *in vitro* human teeth and the corresponding refractive index profiles.

2 All-Fiber OCT System

The OCT system utilizes the principle of low-coherence interferometry with a broadband light source to obtain high spatial resolution. To overcome the polarization sensitivity commonly found in all-fiber OCT systems, we developed a polarization-insensitive scheme. Figure 1 is the schematic of our all-fiber polarization-insensitive OCT system.

The system uses a super luminescent diode (SLD) with a 50-nm FWHM bandwidth and a 1310-nm center wavelength as a light source, resulting in a free-space coherence length of 15 μm. We choose 1310 nm because teeth are a highly scattering tissue with their maximum penetration at 1310 nm. Near-infrared light at 1310 nm is well suited for the detection and imaging of interproximal caries lesions.[10] Light is delivered to the sample by a gradient index (GRIN) lens with a 3-mm focal length. The reflected light from the exit surface of the GRIN lens is used as the reference light. One arm of the interferometer consists of a fiber stretcher-based scanning optical delay line to scan the optical path delay and a variable delay line (VDL) to match the optical length between the two interferometer arms. A Faraday rotator mirror is placed at each end of both interferometer arms to eliminate polarization fluctuations in the single-mode fiber. Such an arrangement completely eliminates polarization sensitivity, even when the sample arm and the interferometer arms are perturbed. The balanced detector receives the interference signal, and the data acquisition (DAQ) card collects the data and transmits them to the computer. A 1-D translation stage driven by a stepper motor is used for transverse scanning of the sample.

3 Description and Validation of the Path-Length Matching Method

Since the time-domain OCT described in Fig. 1 is based on broadband interferometry, it directly measures the group delay
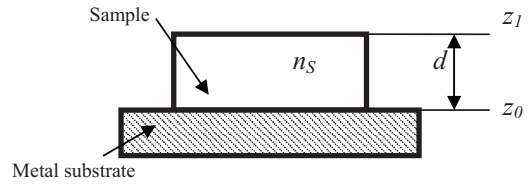
Fig. 2 Schematic diagram of the sample on a metal plate.

of the sample. If the thickness of the sample is known, the group refractive index can be calculated from the group delay. The actual group refractive index n_g and phase refractive index n_p have the following relationship:

$$n_g = n_p - \lambda_0 \left(\frac{dn_p}{d\lambda} \right)_{\lambda_0},\qquad(1)$$

where λ_0 is the center wavelength of the incident light. In practice, the derivative of the phase refractive index as a function of wavelength $dn_p/d\lambda$ is small. For example, the phase refractive index of water at 1300 nm deviates from the group refractive index by only 1.6%.[11] Therefore, we can ignore $dn_p/d\lambda$ and take the measured group refractive index of the sample as the phase index.

To measure the refractive index of a sample, we first place the sample on a metal (unpolished aluminum) plate and then acquire the OCT images. Figure 2 shows a schematic diagram of the sample on the metal plate, where the vertical position of the metal plate's reflection surface is z_0, the vertical position of the sample surface is z_1, the thickness of the sample is d, and the refractive index of the sample is n_S.

Figure 3(a) is a 2-D OCT image (B-scan) of a glass slide on the metal plate that shows the change in the metal plate's vertical position caused by the glass slide. The left portion of the image shows the position of the metal plate without the glass slide present, while the right portion shows its position with the glass slide. The upper surface position of the glass also can be seen clearly. As expected, the depth of the metal plate increases when the glass slide is on top (the position of the metal plate surface changes from z_0 to z_0'), which results from the optical path-length increase caused by the relatively large refractive index of the glass (compared with the air). Assuming that the increase in the optical path-length induced by the glass plate (sample) is $z_0 - z_0'$ and the actual thickness of the sample is $z_1 - z_0$, we can obtain the relationship between the thickness and the refractive index of the glass slide (sample):

$$d = z_1 - z_0 = \frac{(z_1 - z_0')}{n_S}.\qquad(2)$$

Therefore, the refractive index of the sample can be obtained from Eq. (2) as

$$n_S = \frac{z_1 - z_0'}{z_1 - z_0}.\qquad(3)$$

Figure 3(b) is a 1-D OCT image (A-scan) derived from Fig. 3(a). The dotted line is the reflected light from the surface of the metal plate without the sample (glass slide), and its posi-

(a)

(b)
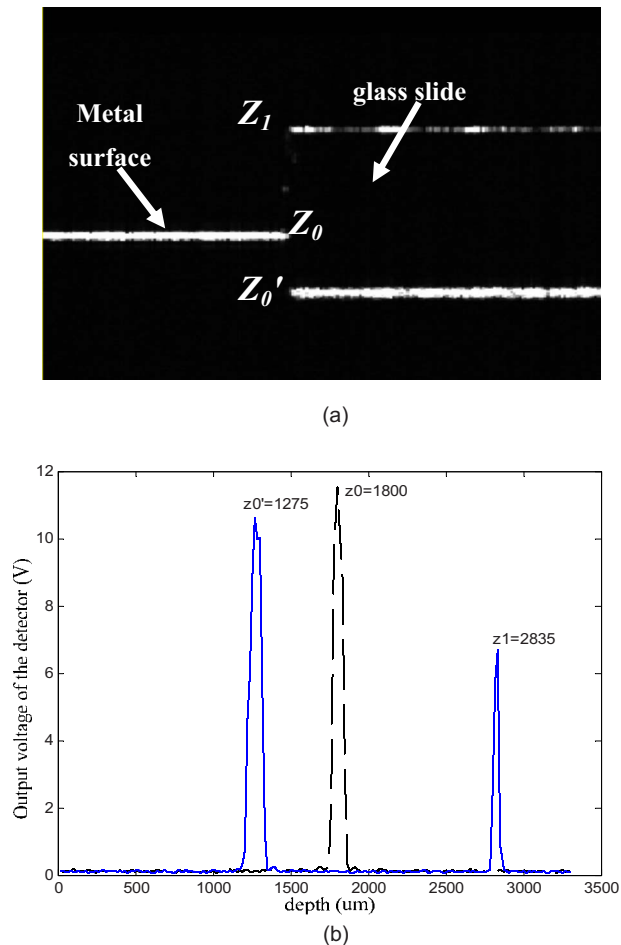
Fig. 3 OCT image of the glass slide: (a) 2-D OCT image of the metal substrate and the glass slide; (b) 1-D OCT image of the metal substrate and the glass slide.

tion is z_0. The solid lines are the reflected light from the upper surface of the sample and the metal plate whose positions are z_1 and z_0', respectively. By Substituting of the values of z_0, z_0', and z_1 into Eqs. (2) and (3), we can obtain the refractive index (n_S) and the thickness (d) of the glass slide to be $n_S = 1.5072$ and $d = 1.035$ mm. For reference, the refractive index of a common glass slide is 1.515 (Ref. 12) and its thickness measured with a vernier caliper is 1.04 mm. Both the index and the thickness are sufficiently close to the values obtained with the OCT method to validate the method's correctness (the errors in index and thickness are 0.8% and 0.5%, respectively).

Note that at 1310 nm, the attenuation of light inside teeth is primarily from scattering, and the absorption is negligible.[10,13] Consequently, the imaginary part of the index of refraction can be ignored. In addition, our method is based on the phase measurement of interfering beams, and there are no apparent attenuation variations within the bandwidth of the SLD source used in the experiment[14]; therefore, any absorption or imaginary part of the index will have little impact on the measurement results.
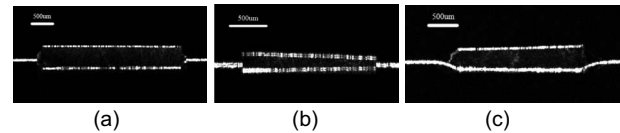
Fig. 4 OCT image of *in vitro* human teeth slices: (a) OCT image of the enamel slice; (b) OCT image of the dentin slice; (c) OCT image of the cementum slice.

4 Results of Teeth Measurement

We measured the enamel, dentin, and cementum of *in vitro* human teeth. In the experiment we first cut and polished freshly removed teeth into thin slices with a slice thickness of 300 to 400 μm, and then placed each tooth slice onto the metal plate to replace the glass slide in Fig. 2. When not in use, these tooth slices were kept in distilled water. Finally, we took B-scan OCT images of the tooth slices placed on the metal plate. The results are shown in Fig. 4. Figures 4(a)–4(c) are the OCT images of an enamel slice, a dentin slice, and a cementum slice, respectively.

We measured 20 samples of the *in vitro* human tooth slices separately, and the resulting refractive indices of the enamel, the dentin, and the cementum were 1.631 ± 0.007, 1.540 ± 0.013, and 1.582 ± 0.010, respectively. In Refs. 15 and 16, the refractive indices of enamel and dentin were 1.60 to 1.65 and 1.50 to 1.55, respectively. Thus our measurement results were consistent with those of Refs. 15 and 16, but with much better accuracy. As reported in Ref. 5, the ranges of refractive index of noncarious and carious enamels are 1.623 ± 0.005 and 1.628 ± 0.004 respectively at the wavelength of 577 nm. We expect the index difference between the noncarious and carious enamels to be similar at 1310 nm and that the resolution of our measurement method is sufficient to detect the changes in refractive index caused by caries. We are currently performing further experiments to measure the indices of noncarious and carious enamels at 1310 nm and will publish the results elsewhere. We performed an analysis of variance (ANOVA) using the 20 sets of refractive index data of dentin and cementum to ensure the refractive indices of dentin and cementum had statistically significant differences. We found that the mean within-group variance of dentin and cementum was 0.000039297 and the variance of the group means was 0.017736731. The corresponding F-test (the ratio of variance of the group means and mean within-group variance) was 451.35, well above the required F-test of 7.35 from the ANOVA look-up table. Therefore, we are certain that the measured indices of dentin and cementum were statistically different.

We did not take the polarization effect into account in the measurements so the resulting data are the average of ordinary and extraordinary indices. Further polarization-sensitive OCT measurements are under way to separately measure both indices.

Figure 5(a) is a photographic image of an *in vitro* tooth slice subject to refractive index measurement. We took a B-scan along the direction marked with a white line in Fig. 5(a) and obtained the 2-D OCT image shown in Fig. 5(b). Using the path-length matching method described above, we obtained the refractive index distribution profile shown in Fig.

(a)

(b)

(c)
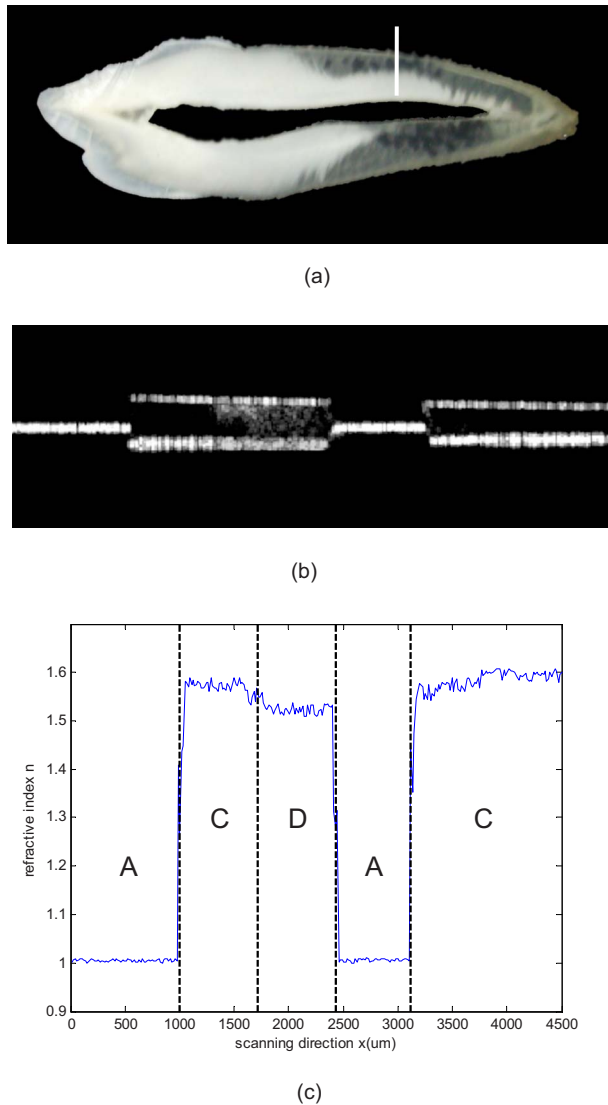
Fig. 5 Refractive index profile of a tooth slide: (a) image of the tooth slice; (b) 2-D OCT image of the tooth slice; (c) refractive index distribution of a tooth slice in (a). A: air; C: cementum; D: dentin.

5(c) along the scan direction by taking each axial scan (A-scan) information [vertical position information in Fig. 5(b)]. One can clearly see from Fig. 5(c) the changes in the refractive index along the scan direction: from the air (with a refractive index of 1) to the cementum (refractive index around 1.58), to the dentin (refractive index around 1.54), and then to the cavum of a pulp cavity (refractive index of 1), and finally to the cementum of the lower side.

5 Summary

We developed a path-length matching method for accurately and quickly measuring the refractive index and index profile across a tooth with a single OCT B-scan. With this method, we obtained the refractive indices of the enamel, the dentin, and the cementum of *in vitro* teeth using 20 different tooth slice samples. We also obtained the refractive index distribution profile of the *in vitro* human teeth. Such an accurate determination of a tooth's refractive indices at different locations is important for the early diagnosis of dental caries that may cause local changes in the refractive index. Equipped with this tool, we can quantitatively study the changes in the refractive index induced by caries and dental decay in detail and relate the data to the early diagnosis of dental caries.

References

1. D. Huang, E. A. Swanson, C. P. Lin, J. S. Schuman, W. G. Stinson, W. Chang, M. R. Hee, T. Flotte, K. Gregory, C. A. Puliafito, et al., "Optical coherence tomography," *Science* **254**(5035), 1178–1181 (1991).
2. B. W. Colston, Jr., M. J. Everett, U. S. Sathyam, L. B. DaSilva, and L. L. Otis, "Imaging of the oral cavity using optical coherence tomography," *Monogr. Oral Sci.*, **17**, 32–55 (2000).
3. A. Baumgartner, S. Dichtl, C. K. Hitzenberger, H. Sattmann, B. Robl, A. Moritz, A. F. Fercher, and W. Sperr, "Polarization-sensitive optical coherence tomography of dental structures," *Caries Res.* **34**(1), 59–69 (2000).
4. B. T. Amaechi, S. M. Higham, A. G. Podoleanu, J. A. Rogers, and D. A. Jackson, "Use of optical coherence tomography for assessment of dental caries: quantitative procedure," *J. Oral Rehabil.*, **28**(12), 1092–1093 (2001).
5. F. C. Besic, and M. R. Wiemann, Jr., "Dispersion staining, dispersion, and refractive indices in early enamel caries," *J. Dent. Res.* **51**(4), 973–985 (1972).
6. M. Haruna, M. Ohmi, T. Mitsuyama, H. Tajiri, H. Marumaya, and M. Hashimoto, "Simultaneous measurement of the phase and group indices and the thickness of transparent plates by low coherence interferometry," *Opt. Lett.*, **23**(12), 966–968 (1998).
7. G.-J. Song, X.-Z. Wang, H.-W. Ren, W.-Z. Zhang, L.-Y. Zhang, and Z.-J. Fang, "Simultaneous measurements of the thickness and refractive index of microstructures in obscure specimen by optical coherence tomography," *Optik (Jena)* **111**(12), 541–543 (2000).
8. G. J. Tearney, M. E. Brezinski, J. F. Southern, B. E. Bouma, M. R. Hee, and J. G. Fujimoto, "Determination of the refractive index of highly scattering human tissue by optical coherence tomography," *Opt. Lett.*, **120**(21), 2258–2260 (1995).
9. J. Kim, D. P. Dave, C. G. Rylander, J. Oh, and T. E. Milner, "Spatial refractive index measurement of porcine artery using differential phase optical coherence microscopy," *Lasers Surg. Med.*, **38**(10), 955–959 (2006).
10. R. S. Jones, G. D. Huynh, G. C. Jones, and D. Fried, "Near infrared transillumination at 1310 nm for the imaging of early dental decay," *Opt. Express*, **11**(18), 2259–2265 (2003).
11. G. M. Hale and M. R. Querry, "Optical constants of water in the 200-nm to 200-μm wavelength region," *Appl. Opt.* **12**(3), 555–563 (1973).
12. M. Bass, *Handbook of Optics*, 2nd ed., vol. 1, p. 43.21, McGraw-Hill, New York (1995).
13. D. Fried, R. E. Glena, J. D. B. Featherstone, and W. Seka, "Nature of light scattering in dental enamel and dentin at visible and near-infrared wavelengths," *Appl. Opt.* **34**(7), 1278–1285 (1995).
14. J. M. Schmitt, "Optical coherence tomography (OCT): A review," *IEEE J. Sel. Top. Quantum Electron.*, **5**(4), 1205–1215 (1999).
15. A. Kienle, R. Michels, and R. Hibst, "Magnification—A new look at a long known optical property of dentin," *J. Dent. Res.* **85**(10), 955–959 (2006).
16. M. Ohmi, Y. Ohnishi, K. Yoden, and M. Harunai, "*In vitro* simultaneous measurement of refractive index and thickness of biological tissue by the low coherence interferometry," *IEEE Trans. Biomed. Eng.*, **47**(9), 1266–1270 (2000).